Available online at www.sciencedirect.com
ScienceDirect
International Journal of Thermal Sciences 46 (2007) 67–75
International Journal of Thermal Sciences
www.elsevier.com/locate/ijts

Gas–solid turbulent flow and heat transfer with collision effect in a vertical pipe

M. Saffar-Avval [a,*], H. Basirat Tabrizi [a], Z. Mansoori [b], P. Ramezani [a]

[a] *Department of Mechanical Engineering, Amirkabir University of Technology, PO Box 15875-4413, Tehran, Iran*
[b] *Energy Research Center, Amirkabir University of Technology, PO Box 15875-4413, Tehran, Iran*

Received 10 September 2005; received in revised form 4 February 2006; accepted 3 April 2006

Available online 5 June 2006

Abstract

A turbulent gas–solid suspension upward flow in a vertical pipe is simulated numerically using Eulerian–Lagrangian approach. Particle–particle and particle–wall collisions are simulated based on deterministic approach. The influence of particle collisions on the particle concentration, mean temperature and fluctuating velocities are investigated. Numerical results are presented for different values of loading ratios. The profiles of particle concentration, mean velocity and temperature are shown to be flatter by considering inter-particle collisions, while this effect on the gas mean velocity and temperature is not significant. It is demonstrated that the effect of inter-particle collisions have a dramatic influence on the particle fluctuation velocity. It is shown that the profiles of particle concentration and particle velocity are flattened due to inter-particle collisions and this effect becomes more pronounced with increasing loading ratio. Also, the attenuation of turbulence by inter-particle collisions in the core region of the pipe is increased by increasing loading ratio.

Keywords: Gas–solid flow; Turbulence; Eulerian–Lagrangian approach; Particle collisions; Heat transfer

1. Introduction

Gas–solid turbulent flows are involved in numerous industrial processes such as pneumatic transport of particulate materials, gasification and environmental pollution. In many cases, the solid fraction is high, thus inter-particle collisions must be taken into account. Additionally, the particle–wall collisions have significant effect on the characteristics of the dispersed phase even in dilute suspensions. These collisions largely modify the flow structure and consequently have a considerable effect on the transport phenomena (Louge and Yusof [1]).

Inter-particle collisions can be computed either deterministically or stochastically. A deterministic method without coupling between the phases was used by Tanaka and Tsuji [2] in a horizontal pipe and effect of inter-particle collisions was reported. Sommerfeld [3] performed a stochastic method without coupling between phases in a horizontal channel and proved that the particle collisions have a significant effect on the particle velocity fluctuation field. Sundaram and Collins [4] considered a four way modeling using Direct Numerical Simulation (DNS) for an isotropic turbulence including the effect of inter-particle collisions to study the turbulence modulation. They found that the rate of viscous dissipation of turbulent energy is enhanced by particles. But the differences of the flow fields with and without considering the effect of inter-particle collision were not examined.

Wassen and Frank [5] investigated the cluster formation in a horizontal channel by applying a stochastic model. They showed that particle–particle interactions have a significant effect on the concentration distribution at moderate to high loading ratios and they tend to enhance the formation of particle cluster for high loading ratios.

Four-way coupling simulation was performed in a fluidized bed by Helland et al. [6]; the influence of the inter-particle collision characteristic on the cluster structure was reported.

Yamamoto et al. [7] performed four way coupled simulation of downward gas–solid flow in a vertical channel considering inter-particle collisions simulated by a deterministic method.

* Corresponding author. Tel.: +98 21 66405844; fax: +98 21 66419736.
E-mail address: mavval@aut.ac.ir (M. Saffar-Avval).

1290-0729/$ – see front matter
doi:10.1016/j.ijthermalsci.2006.04.001

Nomenclature

A_P	particle surface	
c_P	specific heat	$\mathrm{J\,kg^{-1}\,^\circ C^{-1}}$
c_d	drag coefficient	
D	pipe diameter	m
d_p	particle diameter	m
e	restitution coefficient	
f	friction coefficient	
G	relative velocity vector	
g	gravity acceleration	$\mathrm{m\,s^{-2}}$
h_p	heat transfer coefficient	$\mathrm{W\,m^{-2}\,^\circ C^{-1}}$
k	turbulent kinetic energy	$\mathrm{m^2\,s^{-2}}$
K_g	gas heat conductivity	$\mathrm{W\,m^{-1}\,^\circ C^{-1}}$
m	particle mass	kg
Nu	Nusselt number, $= Dh_P/K_g$	
P	pressure	$\mathrm{N\,m^{-2}}$
Pr	Prandtl number, $= \mu c_P/K_g$	
Pr_t	turbulent Prandtl number, $= \nu_t/\alpha_t$	
r	radial coordinate	
Re	Reynolds number, $= \frac{DV\rho}{\mu}$	
T	mean temperature	°C
U	mean axial gas velocity	$\mathrm{m\,s^{-1}}$
u'	velocity fluctuation	$\mathrm{m\,s^{-1}}$
u^*	friction velocity	$\mathrm{m\,s^{-1}}$
V	mean radial gas velocity	$\mathrm{m\,s^{-1}}$
v_c	particle relative velocity	$\mathrm{m\,s^{-1}}$
x	vertical coordinates	m
y	distance from wall	m
z	solid loading ratio	
X, Y, Z	coordinate system (Fig. 1)	

Greek symbols

α	thermal diffusivity	$\mathrm{m^2\,s^{-1}}$
α_t	thermal eddy diffusivity	$\mathrm{m^2\,s^{-1}}$
β_1, β_2	contact angle	
$\varepsilon_X, \varepsilon_Z$	directional cosine	
ε	dissipation rate of turbulent kinetic energy	$\mathrm{m^2\,s^{-3}}$
ϕ	solid volume fraction	
μ	viscosity	$\mathrm{kg\,m^{-1}\,s^{-1}}$
ν	kinematic viscosity	$\mathrm{m^2\,s^{-1}}$
ν_t	eddy viscosity	$\mathrm{m^2\,s^{-1}}$

Subscripts and superscripts

c	contact
f	fluid
g	gas
n	normal component
p	particle
t	tangential component
u	velocity
w	wall
$\bar{x}$	average quantity
x'	fluctuating quantity
0	before collision

They investigated the effect of inter-particle collisions on the flow field and showed that inter-particle collisions make profile of the particle concentration much flatter.

Sommerfeld [8] investigated the motion of particles in a horizontal channel flow with the effect of wall collisions, wall roughness and inter-particle collisions. He used predetermined flow and turbulence fields, and neglected the effect of particles on the gas flow field. He demonstrated that both effect, i.e. wall roughness and inter-particle collisions have a dramatic influence on the particle behavior in a horizontal fully developed channel flow.

Experimental and numerical investigation of gas–solid collisional flow of large spherical particles in a vertical convergent channel was carried out by Fohanno and Oesterle [9]. The effect of the particle collisions on the particle characteristics has been observed.

In spite of a large number of research works on gas–solid flow field, less attention has been paid to heat transfer in gas–solid flow, while the heat transfer is important in combustion phenomena, heat exchanger and drying technology. Mansoori et al. [10] showed that the particle interactions and collisions could markedly influence the particle thermal fluctuation intensity. In a four way interaction Eulerian–Lagrangian model, Mansoori et al. [11] computed the inter-particle contact heat transfer in turbulent gas–solid flow using a deterministic kinetic model. It is shown that inter-particle collision amplifies the effect of solid phase to decrease temperature intensity near the wall and increase it near the pipe center line region.

The stochastic model of particle to particle heat transfer is presented by Mihalyko et al. [12] using a simple kinetic model with random parameters. A population balance model was developed for describing particle to particle heat transfer during collision.

An Eulerian–Lagrangian approach is used to model turbulent gas solid in heated pipe by Chagras et al. [13]. The particle–particle collision has been found to increase the overall heat transfer as much as 8% in vertical pipe gas–solid flow.

The effect of particle collisions has been studied in the fully developed flow by Mansoori et al. [10,11,14]. Their model considered the thermal turbulent field characteristics and included k_θ–τ_θ equation model, in addition the k–τ model for the two-way interaction of two-phase flows. Also, the obtained results showed that the deeper study of particle collision effects on flow field is necessary. Hence, numerical investigation is carried out in the developing region in order to improve our knowledge of particle collision.

In this study, an extension of inter particle collision effect on turbulent heat transfer is presented using a four-way interaction model for gas–solid flows using an Eulerian–Lagrangian approach. Inter-particle collision is treated by the deterministic method. The closure is sought by using k–ε. The influence of particle collisions on the solid fraction, particle velocity, gas

and particle turbulence intensity and heat transfer in a riser are studied. The effects of particle–particle and particle–wall collisions on the flow and temperature fields in a developing vertical pipe for different loading ratios are investigated.

2. Model formulation

The mathematical model of non-isothermal turbulent gas–solid flow in a vertical pipe was developed by using an Eulerian–Lagrangian approach. The gas flow is assumed to be steady, axi-symmetric and incompressible while the solid phase is modeled by Lagrangian simulation. The resulting equation system is closed by means of standard k–ε model [15], while the thermal problem is solved using a turbulent Prandtl number expression by Kays [16] for the closure.

2.1. Gas phase simulation

The governed form of the equations of continuity, momentum and k–ε for a steady axi-symmetric gas flow in cylindrical coordinates may be written as:

$$\frac{\partial}{\partial x}\big((1-\phi)U\Phi\big)+\frac{1}{r}\frac{\partial}{\partial r}\big((1-\phi)rV\Phi\big) = \frac{\partial}{\partial x}\left(\Gamma_\Phi(1-\phi)\frac{\partial\Phi}{\partial x}\right)+\frac{1}{r}\frac{\partial}{\partial r}\left(r\Gamma_\Phi(1-\phi)\frac{\partial\Phi}{\partial r}\right)+S_\Phi \tag{1}$$

Table 1 shows the variables Φ, effective viscosity, source term S for each equation and the various source terms due to the presence of particles. S_u^p and S_v^p represent the momentum exchange between the two phases and S_k^p and S_ε^p are the source terms in k–ε equations. The term $C_{3\varepsilon}$ is ranging from 1.1 to 1.9. Here, a value of 1.8 is used as suggested by Boulet and Moissette [17].

Where, u'_{gi}, u'_{pi} are the fluctuation component of the gas and particle velocities, ϕ' is the particle concentration fluctuation. The fluctuation velocities of gas–particle correlation, $\overline{u'_{pi}u'_{gi}}$ is determined by ensemble and time averaging procedure as is given by Mansoori et al. [11]:

$$\overline{u'_{pi}u'_{gi}}=\frac{1}{N_tN_p}\sum_{l=1}^{N_t}\sum_{n=1}^{N_p}\big[(u_{pi}-U_{pi})(u_{gi}-U_{gi})\big] \tag{2}$$

N_p is the number of particles in the computational cell, N_t is the number of Lagrangian time steps. The correlation between the gas velocity and the particle concentration can be modeled as suggested by Hrenya and Sinclair [18].

$$\overline{\phi'u'_{g1}}\approx\frac{\nu_t}{\sigma_{pg}}\frac{\partial\overline{\phi}}{\partial r},\quad \sigma_{pg}=1 \tag{3}$$

The expressions of the fluctuational components of gas velocity are obtained by a modified Gaussian random field model proposed by Kraichnan [19] which was extended to non-homogeneous flows by Li and Ahmadi [20].

$$u'_g\big(X^+,t^+\big)=\sqrt{\frac{2}{M}}\left\{\sum_{n=1}^{M}U_1\big[\cos\big(K_n.X^++\omega_nt^+\big)\big]\right\} +\sqrt{\frac{2}{M}}\left\{\sum_{n=1}^{M}U_2\big[\sin\big(K_n.X^++\omega_nt^+\big)\big]\right\} \tag{4}$$

Where X^+ denotes the position vector and all quantities are non-dimensionalized with friction velocity u^* and kinematic viscosity.

$$u'^+_{gi}=\frac{u'_{gi}}{u^*},\qquad t^+=\frac{tu^{*2}}{\nu},\qquad x_i^+=\frac{x_iu^*}{\nu}$$
$$U_1=\varsigma_n\times K_n,\qquad U_2=\xi_n\times K_n \tag{5}$$

The component of vectors ς_n, ξ_n and frequencies ω_n are picked independently from a Gaussian distribution with a standard deviation of unity. Each component of K_n is also a Gaussian random number with a standard deviation of 1/2. In Eq. (4) M is the number of terms in the series. Here $M=100$ is used as suggested by Li and Ahmadi [20]. This equation generates an isotropic homogeneous turbulence and for application to

Table 1
Terms in general equation

Φ	Γ_Φ	S_Φ
1	0	0
U	$(\nu+\nu_t)$	$-(1-\phi)/\rho\frac{\partial p}{\partial x}-(1-\phi)g+S_u^p$
V	$(\nu+\nu_t)$	$-(1-\phi)/\rho\frac{\partial p}{\partial r}-2(1-\phi)(\nu+\nu_t)\frac{V}{r^2}+S_v^p$
k	$(\nu+\frac{\nu_t}{\sigma_k})$	$(1-\phi)(G-\varepsilon)+S_k^p$
ε	$(\nu+\frac{\nu_t}{\sigma_\varepsilon})$	$\frac{\varepsilon}{k}(1-\phi)(C_{\varepsilon1}G-C_{\varepsilon2}\varepsilon)+S_\varepsilon^p$
T	$(\alpha+\alpha_t)$	S_t^p

$\nu_t=c_\mu\frac{k^2}{\varepsilon}$, $\quad G=(\nu+\nu_t)\big\{2\big[\big(\frac{\partial U}{\partial x}\big)^2+\big(\frac{\partial V}{\partial r}\big)^2\big]+\big[\big(\frac{\partial U}{\partial r}+\frac{\partial V}{\partial x}\big)^2\big]\big\}$

$\alpha_t=\nu_t/Pr_t$, $\quad Pr_t=\big\{0.5882+0.228(\nu_t/\nu)-0.0441(\nu_t/\nu)^2[1-\exp(-5.165\nu/\nu_t)]\big\}^{-1}$

$S_u^p=\frac{\rho_p}{\tau_p\rho_g}[\phi(U_p-U_g)]$, $\quad \tau_p=\frac{4}{3}\frac{\rho_pd_p}{\rho_gC_D\overline{|U_p-U_g|}}$, $\quad S_v^p=\frac{\rho_p}{\tau_p\rho_g}[\phi(V_p-V_g)]$

$S_k^p=\frac{-\rho_p}{2\tau_p\rho_g}[\phi(\overline{u'_{gi}u'_{gi}}-\overline{u'_{pi}u'_{gi}})+\overline{\phi'u'_{gi}}(U_p-U_g)]$, $\quad S_\varepsilon^p=C_{3\varepsilon}\frac{\varepsilon}{k}S_k^p$

$S_T^p=\frac{F}{\rho_gC_{pg}}[\phi(T_p-T_g)]$, $\quad F=6Nu_pK_g/d_p^2$

$C_\mu=0.09$; $\quad\sigma_k=1.00$; $\quad\sigma_\varepsilon=1.30$; $\quad C_{1\varepsilon}=1.44$; $\quad C_{2\varepsilon}=1.92$; $\quad C_{3\varepsilon}=1.1$–$1.9$

non-homogeneous flows a scaling method is applied. That is, $u'^{+}_{gi} = u'^{+}_{gi}(X^+, t^+)e_i(X^+)$ in which $e_i(X^+)$ are the shape functions for the axial, vertical and transverse rms velocities [19, 20]. Similar formulation is also used for generating the instantaneous gas temperature fluctuations as described in [14]. The procedure is as the generation of the fluctuational components of gas velocity and the non-dimensioned fluctuation of gas temperature $t'^{I+}_g(\vec{\mathbf{X}}^+, t^+)$ is calculated by:

$$t'^{I+}_g\left(\mathbf{X}^+, t^+\right) = (2/M)^{1/2}\left\{\sum_n^M T_1\left[\cos\left(\vec{\mathbf{K}}_n.\vec{\mathbf{X}}^+ + \omega_n t^+\right)\right]\right\} + (2/M)^{1/2}\left\{\sum_n^M T_2\left[\sin\left(\vec{\mathbf{K}}_n.\vec{\mathbf{X}}^+ + \omega_n t^+\right)\right]\right\} \tag{6}$$

Where, t'^{I+}_g is the local gas temperature fluctuation and is properly non-dimensioned. To generate non-homogeneous fluctuation field a scaling method is applied. That is, $t'^{+}_g = t'^{I+}_g.et^+(y_w)$ in which $et^+(y_w)$ is shape functions [14].

2.2. Particle phase simulation

The motion of each individual particle is subject to Newton's equation of motion. The drag and the gravity forces are considered in this equation. Cao and Ahmadi [21] concluded that the rotational energy of particles is less than 10% of their translational energy even for the case of dense granular flow. Therefore, in the present case of relatively low solid volume fractions, the effect of particle rotation and Magnus lift are neglected.

All particles are considered to have spherical shape with smooth surface. The final form of particle equations can be shown as [22]:

$$\mathrm{d}u_{pi}/\mathrm{d}t = \frac{3c_d\rho_g}{4d_p\rho_p}|u_{gi} - u_{pi}|(u_{gi} - u_{pi}) + g$$
$$\mathrm{d}\vec{X}_{pi}/\mathrm{d}t = \vec{u}_{pi} \tag{7}$$

Where, d_p and u_{pi} are the diameter and the particle velocity component respectively. Wen and Yu [23] suggested the drag coefficient dependency with voidage for non-spherical and high concentration mixtures. In the present calculation, the Drag coefficient is assumed to be independent of the voidage due to the fact that the concentration is too low and particles are at the same size and have a spherical shape. So, the drag coefficient model is used as suggested by Schiller and Nauman [24],

$$c_d = 24Re_p^{-1}\left(1 + Re_p^{0.687}/6\right)$$

u_{gi} is the instantaneous gas velocity and is given by the equation $u_{gi} = U_{gi} + u'_{gi}$. U_{gi}, u'_{gi} are the fluid mean velocity and the fluctuation component generated by Kraichnan [19] model respectively.

The temperature equation of each particle is calculated by:

$$mc_p(\mathrm{d}T_p/\mathrm{d}t) = h_pA_p(T_g - T_p) \tag{8}$$

Where h_P, heat transfer coefficient between gas and particle is given by (Crowe et al. [22]). T_g is the fluid temperature at the particle location. Note that $T_g = \overline{T}_g + t'_g$ here t'_g is generated using the procedure mentioned in Section 2.1. Particle Nusselt number is modeled as: $Nu_p = h_pd_p/K_g = 2 + 0.6Re_p^{0.5}Pr^{0.3}$.

2.3. Collision model

The hard sphere model proposed by Crowe et al. [22] is used to describe a binary, instantaneous and inelastic collision considering friction. The occurrence of collision is checked by the calculation of distance between two particle centers. The rebound velocities are calculated by solving the impulsive equations [22].

$$\mathbf{v}_1 = \mathbf{v}_1^0 - 1/2(1 + e_p)\left(\mathbf{n}.\mathbf{G}^0\right)(\mathbf{n} - f_p\mathbf{t}) \tag{9}$$

$$\mathbf{v}_2 = \mathbf{v}_2^0 + 1/2(1 + e_p)\left(\mathbf{n}.\mathbf{G}^0\right)(\mathbf{n} - f_p\mathbf{t}) \tag{10}$$

Where G, is the relative velocity and the superscript "0" denotes variable before collision occurred. **n**, **t** are the normal and tangential unit vectors as shown in Fig. 1(a). f_p and e_p are the friction and particle–particle restitution factors. The hard sphere wall collision model presented by Crowe et al. [22] is employed. The changes in particle velocities in the XYZ coordinates system (Fig. 1(b)) are as below.

$$\mathrm{v}_X = \mathrm{v}_X^0 + \varepsilon_x f_w(1 + e_w)\mathrm{v}_Y^0 \tag{11}$$

$$\mathrm{v}_Y = -e_w\mathrm{v}_Y^0 \tag{12}$$

$$\mathrm{v}_Z = \mathrm{v}_Z^0 + \varepsilon_Z f_w(1 + e_w)\mathrm{v}_Y^0 \tag{13}$$

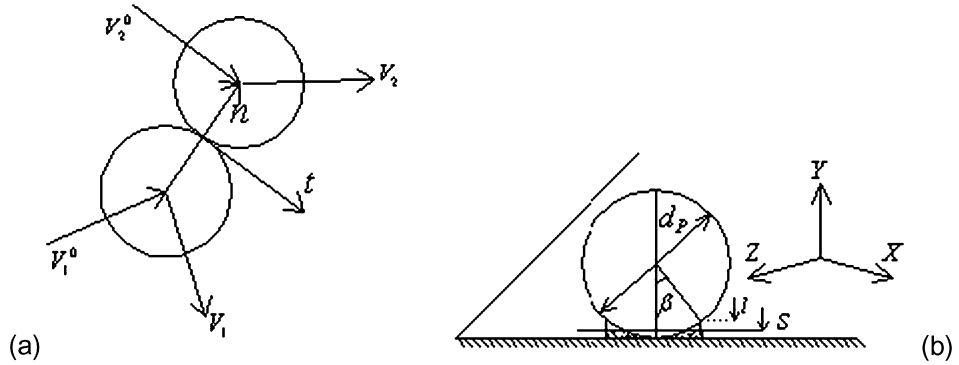

Fig. 1. (a) Schematics of particle–particle collisions and the corresponding pre and post collision velocities. (b) Schematics of particle–wall collisions and the wall coordinate system (X, Z).

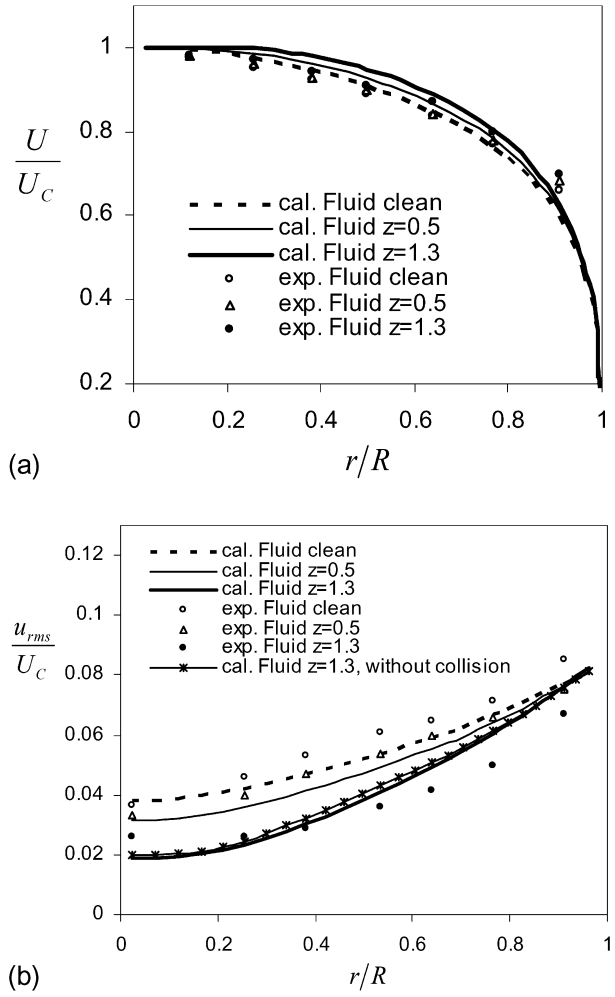

Fig. 2. Comparison with experimental data by Tsuji ($Re = 23\,000$; $d_p = 243$ μm): (a) Velocity profiles; (b) Streamwise gas rms velocity profiles.

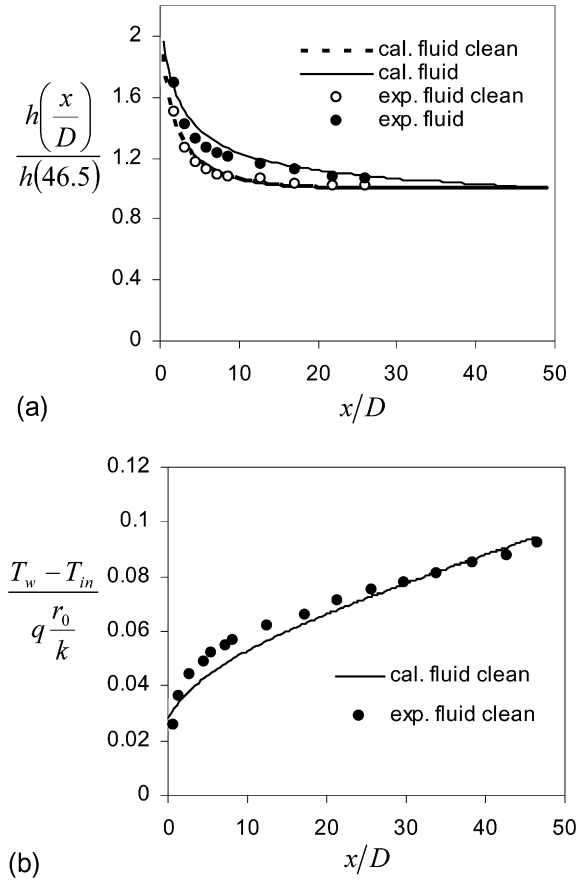

Fig. 3. Comparison with experimental data by Depew and Farbar: (a) Local heat transfer coefficient versus axial distance ($Re = 27\,400$; $d_p = 200$ μm; $z = 0.52$); (b) Dimensionless wall temperature for the pure gas flow versus axial distance ($Re = 13\,500$).

These expressions were derived under the assumption of $-2/[7f_w(e_w+1)] \leqslant V_Y^0/|V^0| < 0$, thus the particles slide during the collision and ε_x, ε_z are the direction cosines of approach velocity in the X–Z plane. f_w and e_w are the particle–wall friction and restitution factors. These parameters are given in Table 1 [25].

3. Numerical simulation

The numerical simulation is performed for a gas–solid particulate flow in a riser of 2 cm diameter and a length of 100 cm. The SIMPLE method of Patankar [26] is used to solve the system of equations for the gas phase. The governing equations are discretized in finite volume form on a staggered grid. The second-order central difference scheme for the pressure gradient and divergence terms and the first order hybrid differencing scheme for the convection terms are used. A classical iterative computation is used to account for the four-way interactions considering not only the two phase interaction, but also the particle–particle collisions.

The particle tracking in Lagrangian simulation is done in a 3D Cartesian coordinate system to avoid the extra terms existing in cylindrical forms of particle motion equations. After each part of the calculation in Lagrangian simulation is completed, the particle location and velocities are transformed to the cylindrical coordinates to be used in the Eulerian part of simulations [11,12].

The governing equations for U_g, k, ε are solved in the core region (between the pipe center and a node located at $y^+ = 30$), while to properly account for the heat transfer, the temperature equation is solved up to the wall, and the heat flux boundary condition given by $-K_g \partial T_g/\partial r|_{r=R} = q_w$. All the calculations are performed with meshes guaranteeing grid-independent results with a cell of sizes 100×30 in the axial and radial direction, respectively. The total number of time steps is chosen to be $N_t = 2000$.

The equations of particle motion are calculated by the fourth-order Runge–Kutta scheme. The Lagrangian time step for solving the particle equations is chosen as described by Lain et al. [27]. The particles are initially distributed randomly across the flow domain to achieve a uniform initial concentration distribution. The initial particle velocity and temperature is chosen as 70% of gas mean velocity and temperature.

The deterministic process is used for simulating interparticle collisions. In the hard sphere model, only binary collision is taken into account. If the distant between particle centers

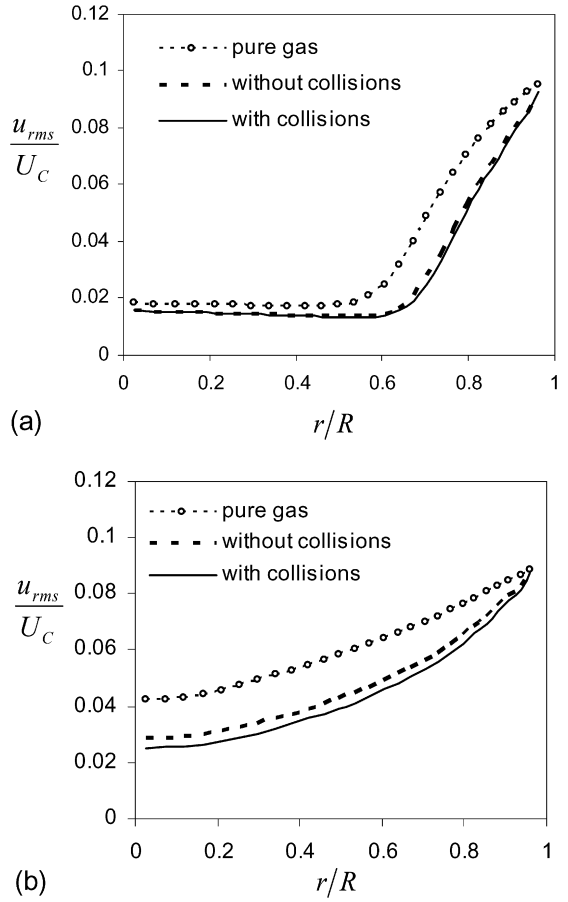

Fig. 4. Streamwise gas turbulence intensity profiles at two locations of the pipe length: (a) $x/D = 10$; (b) $x/D = 50$ ($Re = 14\,000$; $d_p = 300$ μm; $z = 3.5$).

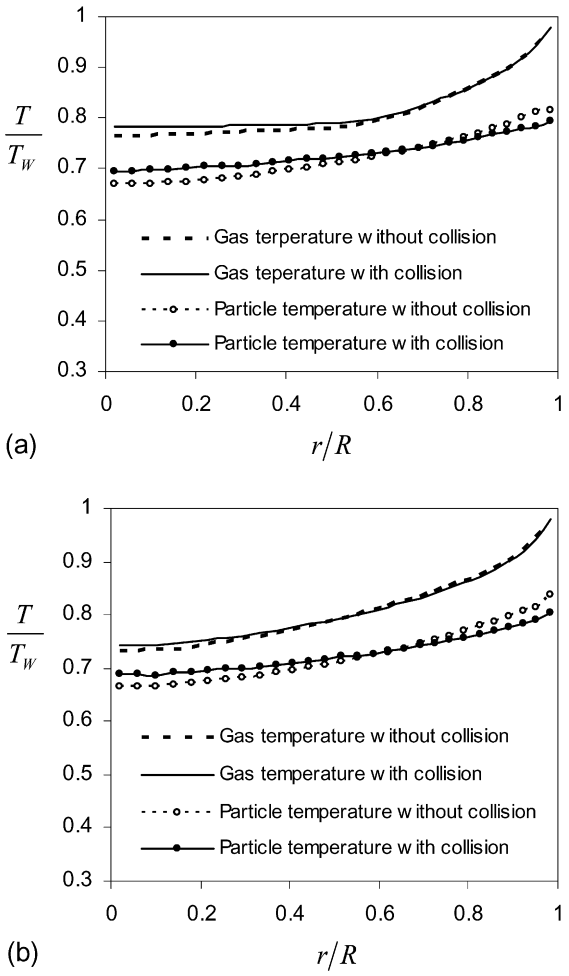

Fig. 5. Temperature profiles at two locations of the pipe length: (a) $x/D = 10$; (b) $x/D = 50$ ($Re = 14\,000$; $d_p = 300$ μm; $z = 3.5$).

is less than the particle diameter then collisions are assumed to be occurred. In order to reduce the required CPU time, a list of neighboring particles is stored for each particle and control of possible collision partners is performed only for the listed neighboring particles. Whenever particle–wall collision is detected, the after wall collision velocities are obtained using Eqs. (11)–(13). Any particle leaves the calculation domain in the axis of symmetry, would be replaced by a new particle entering in the same location but in the opposite direction. This is done to keep the number of particles constant in calculation domain.

4. Numerical validation

4.1. Hydrodynamic characteristics

Experimental data of Tsuji et al. [28] is used to validate the dynamic characteristics. The model and experimental results of velocity and streamwise turbulent intensity profiles are presented in Fig. 2. The case of gas–solid pipe flow with a Reynolds number of 23 000 loaded with polystyrene 243 μm particles with density of 1030 kg m^{-3} is addressed. Velocity profiles are plotted in Fig. 2(a) for loading ratios z (the solid to gas mass flux) of 0.5 and 1.3. The gas velocity is normalized to that at pipe axis. Fig. 2(b) shows the results for gas rms velocity. The lines represent the model results while symbols show the experimental data. A reasonably good agreement with the measurement data is found especially in the core region.

4.2. Thermal characteristic

In order to verify the accuracy of the present model computations are carried out for the status of experimental condition of Depew and Farbar [29] with 200 μm spherical glass and gas Reynolds number of 27 400.

The numerical prediction and experimental data of local heat transfer coefficients are plotted as a function of the axial location along the pipe in Fig. 3(a). The simulation results are slightly above the experimental values in the lower part of the riser. The trend of the experimental results is quite well predicted by model.

The dimensionless tube wall temperature for the pure gas flow versus axial distance is shown in Fig. 3(b). The agreement between numerical and experimental data is good. However, the model predicts slightly lower amounts of the wall temperature in the lower part of the heated section tube.

5. Results and discussion

In this section, the effects of inter-particle collision on the flow field and heat transfer in a vertical pipe is studied. The

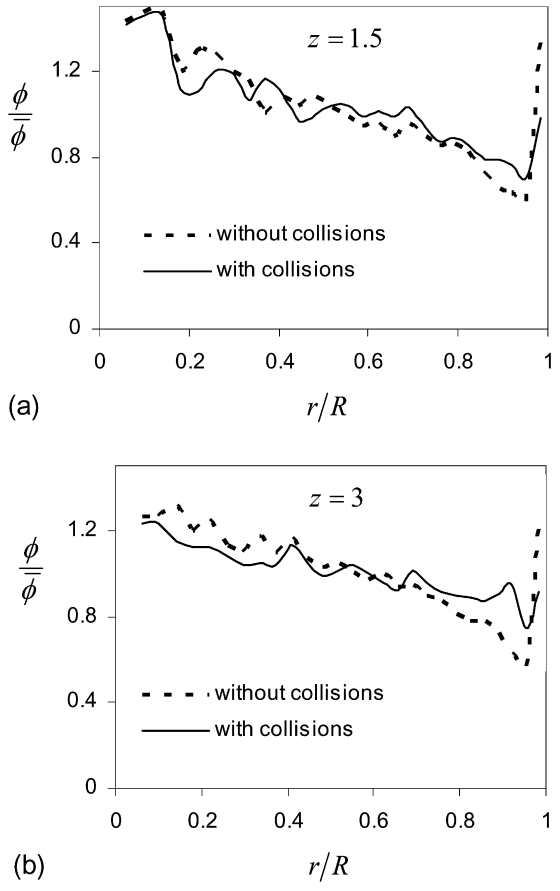

Fig. 6. Solid fraction profile normalized by mean values with and without particle collisions for different loading ratios ($Re = 14\,000$; $d_p = 300$ μm; $\rho_p = 1600$).

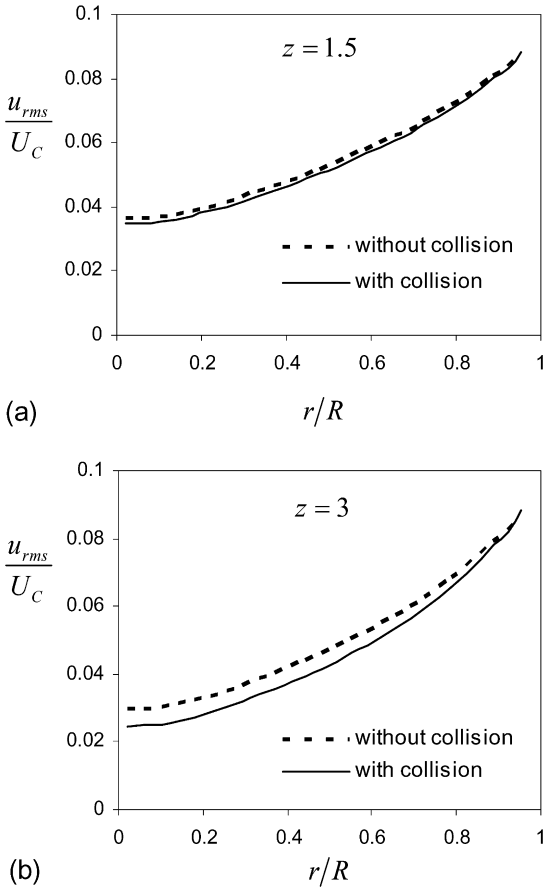

Fig. 7. Streamwise gas turbulence intensity profiles with and without particle collisions for different loading ratios ($Re = 14\,000$; $d_p = 300$ μm; $\rho_p = 1600$).

Table 2
Physical and numerical simulation parameter

Property	Symbol	Value
Pipe sizes	$L \times D$	100×2 cm
Number of grid cell	$N_x \times N_r$	100×30
Reynolds number	Re	14 000
Particle diameter	d_p	300 μm
Particle density	ρ_p	1600
Stokes number	St	42
Restitution coefficient		
(particle–particle)	e_p	0.9
(particle–wall)	e_w	0.95
Friction coefficient		
(particle–particle)	f_p	0.2
(particle–wall)	f_w	0.3
Mass loading ratio	z	1.5, 2.2, 3
Total number of particles	N_p	15 000
Particle time step	Δt	5×10^{-5}

physical and numerical parameters used in this simulation are summarized in Table 2. Particle Stokes number calculated on the center-line and indicates that particles move independently of turbulent eddies.

In order to study the effect of collision in the developing region, two cases with and without considering particle–particle collisions are calculated. Results are illustrated at the two axial positions; $x/D = 10,\ 50$.

Then, the effect of particle collisions on the gas and particle characteristics is analyzed for different values of mass loading ratios in a vertical pipe. The particle concentration, streamwise mean velocity and fluctuation velocity profiles and the gas turbulence intensity are compared for different mass loading ratios in the fully developed region.

5.1. Particle collision effects in developing region

The streamwise turbulence intensity profiles are shown in Fig. 4. The particles suppress the turbulence throughout the pipe section. Inter-particle collisions increase gas turbulence attenuation and this effect is stronger in the core region because energy transferred from turbulence to particles is dissipated by non-elastic collision. The collision effect is higher in the upper part of pipe where the flow moves toward the developed region.

Fig. 5 shows mean gas and particle temperature with and without considering the effect of collision. The results of gas and particle mean velocities are not presented, because the effect of inter-particle collision on the gas and particle mean velocities is similar to that of mean gas and particle temperature. Particle mean temperature profiles with considering the effect of collisions are flatter than those without collisions while gas temperature profiles are unchanged when collisions are taken into account. The particle temperature is increased in the pipe

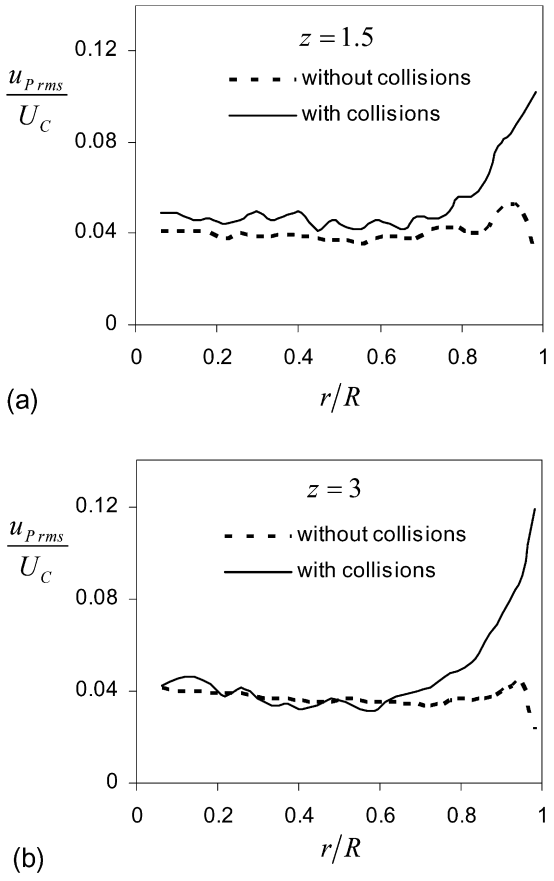

Fig. 8. Streamwise particle turbulence intensity profiles with and without particle collisions for different loading ratios ($Re = 14\,000$; $d_p = 300$ μm; $\rho_p = 1600$).

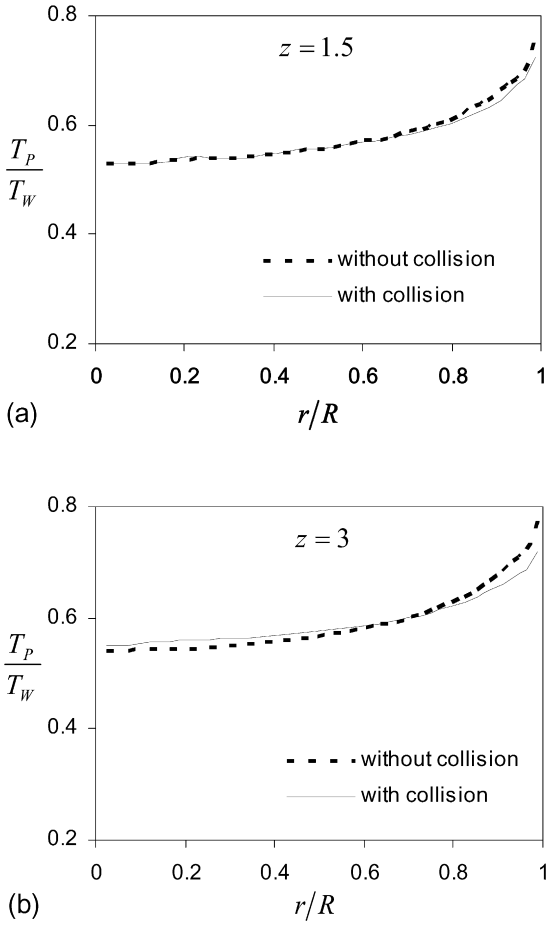

Fig. 9. Particle temperature profiles with and without particle collisions for different loading ratios ($Re = 14\,000$; $d_p = 300$ μm; $\rho_p = 1600$).

core region and is decreased near the wall as a result of collision. This is caused by diffusion of heat across the pipe when inter-particle collisions are considered. That is high temperature particles coming from the near heated wall region reach the core region and therefore transfer their thermal energy into this region.

5.2. Mass loading ratio

This simulation are carried out with a Reynolds number of 14 000 and 300 μm sand particles for different loading ratios. The particle concentration profiles are normalized by mean values for different mass loading ratios and are shown in Fig. 6. The results are demonstrated for both cases: with and without considering particle collisions at the fully developed region of riser. It is shown while the inter-particle collisions are taken into account and the mass loading is increased; particles become more uniformly dispersed across the pipe section. This is caused by increasing particle number density and hence more inter-particle collisions. The high particle concentration in the near wall is reduced due to particle–wall collisions.

The modification of turbulence intensity of the gas phase profiles is shown in Fig. 7 for different mass loading ratios. The turbulence of the gas phase is reduced by inter-particle collisions. This effect is more pronounced for the higher mass loading ratios in the core of the pipe.

In Fig. 8 the variation of the streamwise particle fluctuation velocities are illustrated with different loading ratios. Particle fluctuation velocities are considerably increased near the wall for all loading ratios. The differences between the cases with and without particle collisions are increased with growing loading ratios near the wall. This is caused by lateral dispersion of the particles originating from wall collisions. Also an enhancement of particle fluctuation velocity is seen in the core of the pipe due to the inter-particle collisions.

The effect of inter-particle collisions on the particle temperature profiles normalized by wall temperature is illustrated in Fig. 9. The particle temperature is decreased near the wall as a result of the collision and this effect is more considerable for higher loading ratios.

6. Conclusions

Simulation of gas–solid turbulent upward flow in a vertical pipe was performed by using k–ε turbulence modeling.

Numerical calculations were carried out for different loading ratios. The results indicated that inter-particle collisions affect the flow structure in developing region and the importance of this effect was moderately more when the flow moves upward toward the developed region especially on particle concentration and gas turbulence intensity. It was demonstrated that the

profiles of particle concentration and particle velocity were flattened due to inter-particle collisions. This effect became more pronounced by increasing loading ratios. This was caused by higher particle number densities for smaller particles.

In the near wall region a strong increase of streamwise particle fluctuation profiles has been shown. It was found that the gas turbulence intensity is decreased due to inter-particle collisions and this effect becomes more important by increasing loading ratio.

References

[1] M. Louge, J.M. Yusof, Heat transfer in the pneumatic transport of massive particles, Int. J. Heat Mass Transfer 36 (2) (1993) 265–275.

[2] T. Tanaka, Y. Tsuji, Numerical simulation of gas–solid two phase flow in a vertical pipe: on the effect of inter-particle collision, ASME, FED, Gas–Solid Flows 121, pp. 123–128.

[3] M. Sommerfeld, The importance of ineter-particle collisions in horizontal gas–solid channel flows, in: D.E. Stock (Ed.), Gas–Particle Flows, in: ASME Fluids Engineering Conference, Hiltons Head, USA, FED, vol. 228, ASME, 1995, pp. 335–345.

[4] S. Sundaram, L.R. Collins, A numerical study of the modulation of isotropic turbulence by suspended particles, J. Fluid Mech. 379 (1999) 105–143.

[5] E. Wassen, Th. Frank, Simulation of cluster formation in gas–solid flow induced by particle–particle collisions, Int. J. Multiphase Flow 27 (2001) 437–458.

[6] E. Helland, R. Occelli, L. Tadrist, Computational study of fluctuating motion and cluster structures in gas–particle flows, Int. J. Multiphase Flow 28 (2002) 199–223.

[7] Y. Yamamoto, M. Potthoff, T. Tanaka, T. Kajishima, Y. Tsuji, Large-eddy simulation of turbulent gas–particle flow in a vertical channel: Effect of considering inter-particle collisions, J. Fluid Mech. 442 (2001) 303–334.

[8] M. Sommerfeld, Analysis of collision effects for turbulent gas–particle flow in a horizontal channel: Part I. Particle transport, Int. J. Multiphase Flow 29 (2003) 675–699.

[9] S. Fohanno, B. Oesterle, Analysis of the effect of collisions on the gravitational motion of large particles in a vertical duct, Int. J. Multiphase Flow 26 (2000) 267–292.

[10] Z. Mansoori, M. Saffar-Avval, H. Basirat-Tabrizi, The effect of particle–particle interaction on heat transfer in a horizontal turbulent gas–solid channel flow, in: The ISHMT/ASME Heat and Mass Transfer Conf., India, 2000, pp. 379–384.

[11] Z. Mansoori, M. Saffar Avval, H. Basirat-Tabrizi, G. Ahmadi, Thermomechanical modeling of turbulent heat transfer in gas–solid flows including particle collisions, Int. J. Heat Fluid Flow 23 (2002) 792–806.

[12] Cs. Mihalyko, B.G. Lakatos, A. Matejdesz, T. Blicle, Population balance model for particle to particle heat transfer in gas–solid systems, Int. J. Heat Mass Transfer 47 (2004) 1325–1334.

[13] V. Chagras, B. Oesterlé, P. Boulet, On heat transfer in gas–solid pipe flow: Effects of collision induced alterations of the flow dynamics, Int. J. Heat Mass Transfer 48 (2005) 1649–1661.

[14] Z. Mansoori, M. Saffar-Avval, H. Basirat Tabrizi, G. Ahmadi, Modeling of heat transfer in turbulent gas–solid flow, Int. J. Heat Mass Transfer 45 (2002) 1173–1184.

[15] B.E. Launder, D.B. Spalding, Mathematical Models of Turbulence, Academic Press, New York, 1972.

[16] W.M. Kays, Turbulent Prandtl number—Where are we? Trans. ASME 116 (1994) 284.

[17] P. Boulet, S. Moissette, Influence of the particle-turbulence modulation modeling in the simulation of a non-isothermal gas–solid flow, Int. J. Heat Mass Transfer 45 (2002) 4201–4216.

[18] C.M. Hrenya, J.L. Sinclair, Effect of particle-phase turbulence in gas–solid flows, AIChE Journal 43 (4) (1997) 853.

[19] H. Kraichnan, Diffusion by random velocity field, Phys. Fluids 11 (1970) 22–31.

[20] A. Li, G. Ahmadi, Computer simulation of deposition of aerosols in a turbulent channel flow with rough walls, Aerosol. Sci. Technol. 18 (1993) 11–24.

[21] J. Cao, G. Ahmadi, Gas–particle two-phase turbulent flow in a vertical duct, Int. J. Multiphase Flows 21 (1995) 1203.

[22] C. Crowe, M. Sommerfeld, Y. Tsuji, Multiphase Flows with Droplets and Particles, CRC Press, Boca Raton, FL, 1998.

[23] C.Y. Wen, Y.H. Yu, Mechanics of fluidization, Chem. Engrg. Prog. Symp. Ser. 62 (1966) 100–108.

[24] L. Schiller, A. Nauman, Z. Ver. Dtsch. Ing. 77 (1933) 318–320.

[25] S. Yuu, H. Nishikawa, T. Umekage, Numerical simulation of air and particle motions in group-B particle turbulent fluidized bed, Powder Tech. 118 (2001) 32–44.

[26] S.V. Patankar, Numerical Heat Transfer and Fluid Flow, Hemisphere, New York, 1980.

[27] S. Lain, D. Broder, M. Sommerfeld, Experimental and numerical studies of the hydrodynamics in a bubble column, Chem. Engrg. Sci. 54 (1999) 4913–4920.

[28] Y. Tsuji, Y. Morikawa, H. Shiomi, LDV measurement of an air–solid two-phase flow in a vertical pipe, J. Fluid Mech. 139 (1984) 417–434.

[29] C.A. Depew, L. Farbar, Heat transfer to pneumatically conveyed glass particles of fixed size, in: Trans. ASME J. Heat Transfer C 85 (1963) 164.